Al-Si-Cu alloy enhanced to high-temperature application by nickel addition

J. Camarillo-Cisneros
Laboratory of Computational Physical Chemistry, Facultad de Medicina y Ciencias Biomédicas, Universidad Autónoma de Chihuahua, Chihuahua, México.

R. Pérez-Bustamante
Consejo Nacional de Ciencia y Tecnología-Corporación Mexicana de Investigación en Materiales S.A. de C.V., Eje 126 no. 225, Zona Industrial del Potosí, San Luis Potosí, México.

R. Martínez-Sánchez
Centro de Investigación en Materiales Avanzados, Laboratorio Nacional de Nanotecnología, Chihuahua, México.

Received 14 October 2021; accepted 23 November 2021

The present research evaluates commercial aluminum alloys 319 (AA319) and modified series by Ni additions on microstructure and mechanical properties through x-ray diffraction, electron microscopy, hardness, and tensile tests. All AA319+X%Ni compositions ($x = 0.5$, 1, 2) improved both hardness and UTS at room temperature, $T6$, over-aging, and high-temperature conditions. UTS obtained an improvement of around 30% to $AA319 + 1\%Ni$ and $AA319$+2%Ni relatives to unmodified reference from $T6$ and high-temperature conditions. In addition, Ni increased remarkably the number of θ'-Al_2Cu pairs and reduced their thickness within the aluminum matrix compared to commercial alloy. The synthesis methodology is also adaptable to the current aluminum casting industry, creating the material in ingots and finished products.

Keywords: Al-Si-Cu systems; nickel effect.

DOI: https://doi.org/10.31349/RevMexFis.68.031004

1. Introduction

The use of aluminum alloys is of great interest in automotive and industrial applications that depend on the weight-to-strength ratio [1–3]. Al-Si-Cu systems [4, 5], among them the A319, can further improve their mechanical properties by standard heat treatments [6, 7], by the Al_2Cu (θ') nano-precipitates and Al_2Si (ϵ-Si) micro-precipitates phases [8, 9]. Although improvements in the mechanical performance of Al-Si-Cu alloys due to phase-related changes of θ' after various heat treatments, their engineering applications remain limited to temperatures below 150°C [10]. A necessary additional characteristic to modern applications is lightweight to work at higher temperatures. However, Al-Si-Cu systems can be modified in their chemical composition through additional alloying elements. In this regard, Ni, which generates Al-Ni intermetallic compounds that exhibit high thermal stability and high melting point, is an excellent option for aluminum alloys. It has been reported that additions of 1 to 2% Ni to $2xx$ and $3xx$ series alloys enhance hardness and tensile properties at elevated temperatures [11, 12], due to precipitation of Al_3Ni, Al_3 $(CuNi)_2$, and Al_7Cu_4Ni intermetallics [13, 14]. Specifically, to $AA319$, Ni improved UTS by forming Fe-rich intermetallics, reducing this impurity in the alloy. Fe-Ni intermetallics, as Al_9FeNi, have a relatively high thermal stability at typical temperatures used in $AA319$ heat treatments, so they would not be affected by subsequent heat treatments.

This research studied the Nickel effect as an additional alloying element in aluminum alloy 319 alloys regarding microstructure and mechanical properties in as-cast, $T6$ heat treatment, and overheating conditions.

2. Experimental procedure

The raw materials were commercial $AA319$ and Al-20Ni ($wt.\%$) master alloys. The $AA319$ alloy was melted at 740°C in a graphite crucible using a Lindberg Blue electric furnace. Al-20Ni master alloy was added in different proportions to obtain $+1$, $+1.5$, and +2%Ni modified alloys. Synthesized alloys were degassed for 5 minutes using Ar gas and a graphite propeller at 490 rpm, then 0.33 ($wt.\%$) of Al-5Ti-B grain refiner was added. Table I contains elementary quantifications obtained by inductively coupled plasma-atomic emission spectroscopy.

Mechanical properties were measured by tensile and hardness tests using as-cast and heat-treated samples; this

TABLE I. Chemical compositions obtained by ICP-AES: AA319 corresponds to the commercial alloy until modified compositions correspond to +1, +1.5, and +2 ($wt.\%$) Nickel.

	Si	Cu	Fe	Zn	Mg	Mn	Ni	Al
Al-319	7.94	2.51	0.7	0.39	0.33	0.25	0.04	bal
$+1\%$Ni	7.64	2.2	0.57	0.37	0.33	0.24	1.08	bal
$+1.5\%$Ni	7.47	2.11	0.59	0.37	0.33	0.24	1.59	bal
$+2\%$Ni	7.13	2.1	0.54	0.38	0.31	0.26	2.15	bal

TABLE II. Nomenclature corresponds to $AA319$ and Ni-modified alloys. Tests at ambient temperature correspond to as-cast (AC), solubilized + aging ($T6$), and $over-heating$ at 250°C (OH) conditions. Tensile tests performed at high-temperature conditions over $T6$ samples correspond to 495°C (HT1) and 520°C (HT2).

Sample	Test temperature at 25°C		Test temperature at 250°C	
	Solubilization$_{(5hrs@495°C)}$			Solubilization $_{(3hrs@520°C)}$
	$T6$	OH $_{(45min@250°C)}$	HT1 $_{(45min@250°C)}$	HT2 $_{(45min@250°C)}$
Al-319	A_{T6}	A_{OH}	A_{HT1}	A_{HT2}
+1% Ni	+1%N$_{T6}$	+1%N$_{OH}$	1%N$_{HT1}$	+1%N$_{HT2}$
+1.5% Ni	+1.5%N$_{T6}$	+1.5%N$_{OH}$	+1.5%N$_{HT1}$	+1.5%N$_{HT2}$
+2% Ni	+2%N$_{T6}$	+2%N$_{OH}$	+2%N$_{HT1}$	+2%N$_{HT2}$

last case considered room temperature and 250°C conditions. Regarding room temperature tests, the thermal history of samples includes four categories:

I) As-cast (AC),

II) T_{6-1} consisted of solubilization at 495°C for five hours, quenching in the water at 60°C and aging at 220°C for three hours.

III) T_{6-2} consisted of solubilization at 520°C for three hours and the same quenching and aging.

IV) Overheating condition (OH) obtained by T_{6-1} samples subject to 250°C for 45 minutes, then cool at room temperature.

V) High temperature of 250°C after 45 min for temperature homogenization test in T_{6-1} and T_{6-2}.

A Panalytical X'Pert PRO diffractometer was used for the initial characterization by X-ray diffraction (XRD) technique with Cu radiation at 40 kV and 35 mA. Samples prepared by conventional metallographic techniques and chemically attacked using $20_{HClO4}/80_{MeOH}$ were analyzed by scanning electron microscopy (SEM), JEOL 5800-LV operated at 20 kV. In the transmission electron microscopy (TEM), we used PHILIPS CM-200, and JEOL JEM2200FS operated at 200 kV. Metallographic preparation was based on electropolishing at -30°C using $30_{HNO3}/70_{MeOH}$ electrolyte solution and 20 V. Samples to tensile tests were manufactured according to the E8-ASTM standard and tested in an Instron-337 universal machine at 0.1 mm/s. Evaluation hardness in a *Rockwell-Wilson* tester was done and reported on the *Rockwell-B* scale.

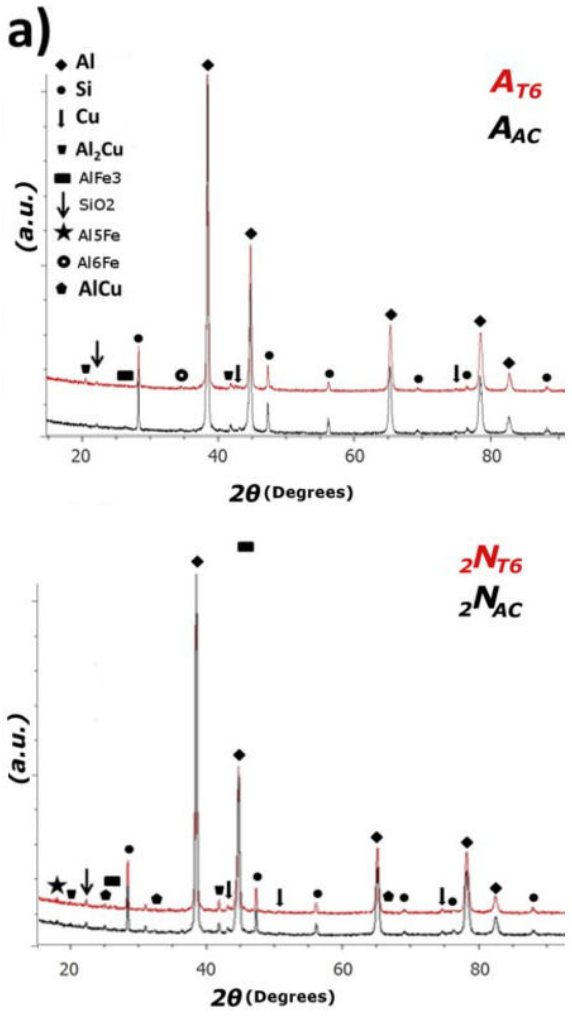

FIGURE 1. X-ray diffraction patterns for as-cast and $T6$ conditions: a) Al-319, b) +2%Ni. Crystal structures were determined using the Rietveld method.

3. Results

In Fig. 1, XRD patterns show the peaks corresponding to the significant constitutive elements Al, Si, and Cu. Quantification of metallic-Cu was slightly higher in $T6$ than as-cast. The Ni addition does not change this behavior. Cu clusters suffered significant changes due to heat treatment, where no significant variations were observed compared to the AA319 and $AA319$ + 2%Ni. The Al_2Cu phase was observed in $AA319$ after $T6$ heat treatment. An unexpected $AA319$ + 2%Ni Al_2Cu phase was obtained in a lower concentration.

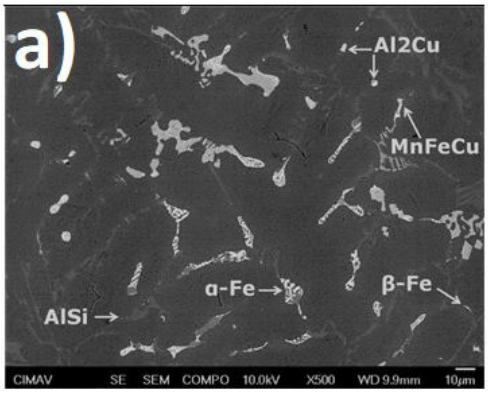

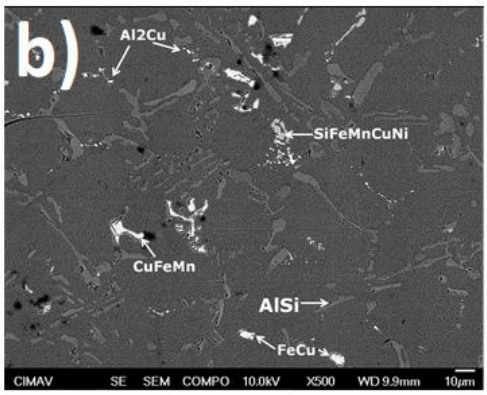

c) EDS from a)

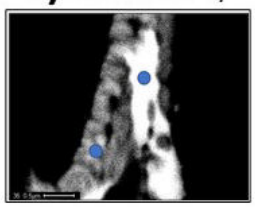

Element	Gray phase		Clear phase	
	Wt%	*At%*	*Wt%*	*At%*
AlK	51.90	61.98	53.66	68.30
SiK	18.92	21.71	07.26	08.88
MnK	06.54	03.84	03.88	02.42
FeK	12.34	07.12	09.18	05.65
NiK	03.07	01.69	15.40	09.01
CuK	07.23	03.67	10.62	05.74

d) EDS from b)

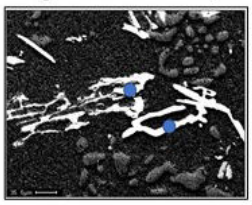

Element	left phase		right phase	
	Wt%	*At%*	*Wt%*	*At%*
AlK	48.77	65.08	37.98	58.17
SiK	06.06	07.77	--	--
MnK	03.82	02.51	--	--
FeK	06.26	04.03	--	--
NiK	15.44	09.47	27.85	19.60
CuK	19.66	11.14	34.17	22.22

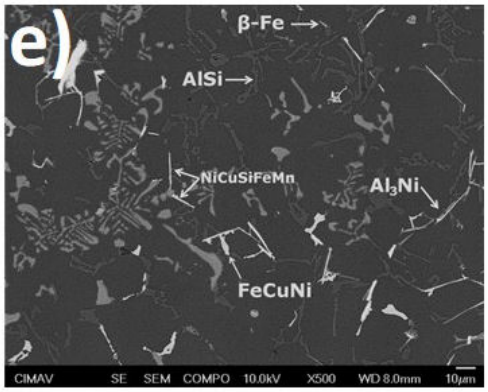

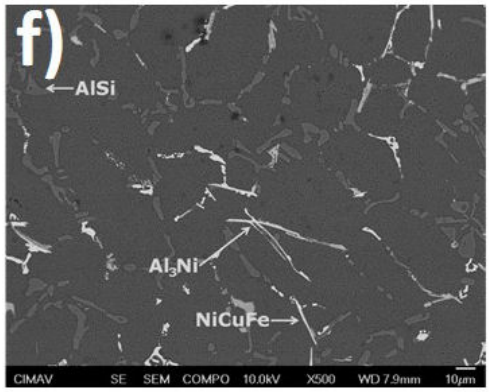

g) EDS from e) and f)

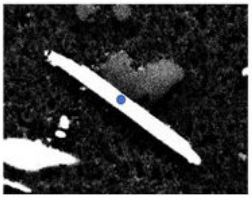

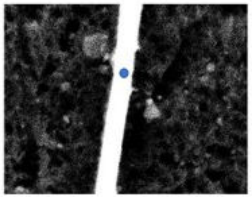

Element	left phase		right phase	
	Wt%	*At%*	*Wt%*	*At%*
AlK	44.80	57.02	62.89	74.59
SiK	17.21	21.04	03.92	04.47
MnK	02.55	01.59	02.10	01.22
FeK	03.69	02.27	02.75	01.58
NiK	20.63	12.06	16.98	09.26
CuK	11.12	06.01	09.25	04.66

FIGURE 2. SEM micrographs of as-cast and $T6$ heat treatment conditions; a) as-cast $AA319$, b) $AA319_{T6}$, c) as-cast $AA319 + 2\%\text{Ni}_{T6}$, d) $AA319 + 2\%\text{Ni}_{T6}$. The EDS results in Figs. c), d), and g) correspond to the representative phases found in more significant quantities in each thermal state and chemical composition.

To $AA319 + 2\%$Ni, additional phases were indexed corresponding to expect AlNi and AlCu. The $T6$ heat treatment does not modify Ni intermetallic compounds because of thermal stability, which is related to an expected increment in the hardness performance.

SEM micrographs (Fig. 2a)) of the as-cast $AA319$ show that α-Al precipitates do not present a clear dendritic arrangement morphology, obtaining a similar microstructural arrangement that the observed for as-cast $AA319 + 2\%$Ni (Fig. 2b)). ϵ-Si precipitates were rounder in shape and smaller than the case of as-cast $AA319 + 2\%$Ni than in commercial $AA319$, while ϵ-Si precipitates appear in block-shape morphology after Ni addition.

Al_2Cu clusters were identified as coarsening particles in the as-cast stage. Intermetallic particles were identified along Al-matrix containing as main elements: Cu, Fe, Mn, and Ni

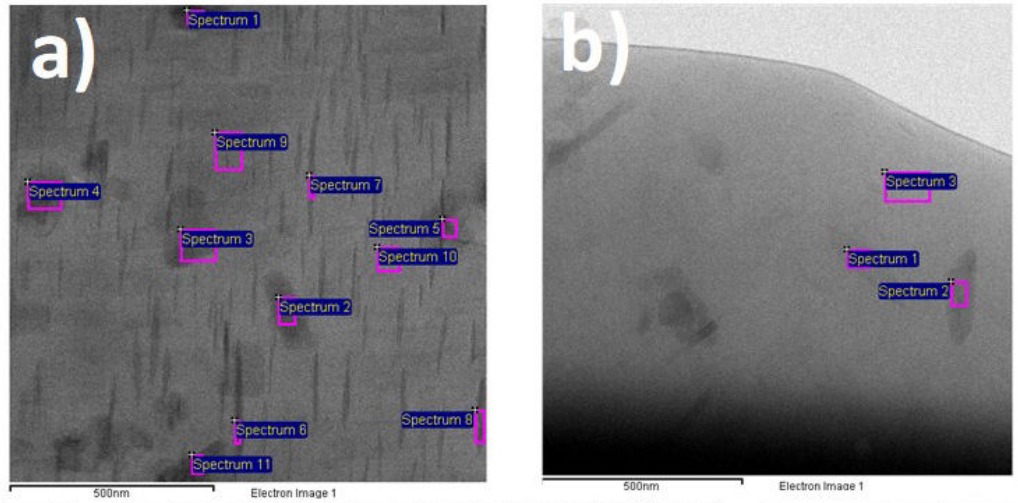

	S-1	S-2	S-3	S-4	S-5	S-6	S-7	S-8	S-9	S-10	S-11
Al	73.81	59.89	6085	56.93	69.75	78.71	84.83	79.07	81.35	83.81	92.0
Si	11.48	3.51	7.60	9.55	8.91	--	--	--	--	--	--
Mn	--	0.97	--	5.48	--	--	--	--	--	--	--
Fe	--	0.55	---	2.45	--	--	--	--	--	--	--
Cu	12.90	33.75	30.12	24.40	20.02	21.29	15.17	20.93	16.03	16.19	7.94
Zn	1.81	1.33	1.43	1.20	1.30	--	--	--	2.62	--	--

	S-1	S-2	S-3
Al	84.41	67.89	92.00
Si	2.29	6.30	2.62
Mn	--	0.96	--
Mg	--	1.28	--
Cu	12.89	22.77	5.39
Zn	0.41	0.80	--

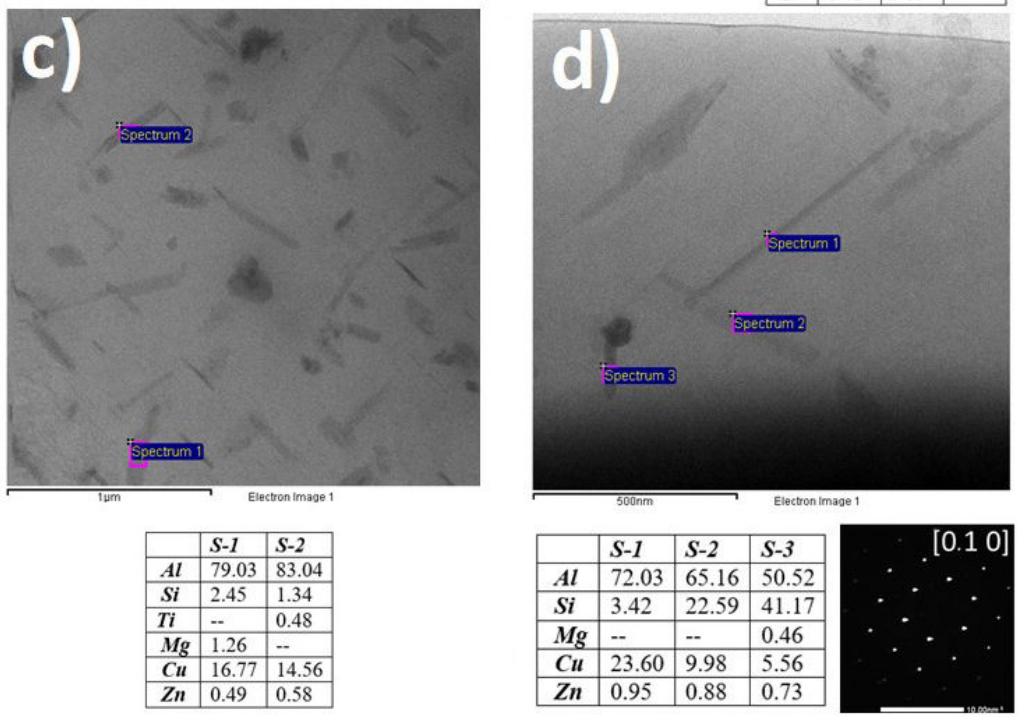

	S-1	S-2
Al	79.03	83.04
Si	2.45	1.34
Ti	--	0.48
Mg	1.26	--
Cu	16.77	14.56
Zn	0.49	0.58

	S-1	S-2	S-3
Al	72.03	65.16	50.52
Si	3.42	22.59	41.17
Mg	--	--	0.46
Cu	23.60	9.98	5.56
Zn	0.95	0.88	0.73

FIGURE 3. TEM micrographs of a) $AA319_{T6}$, b)$AA319_{\text{OH1}}$, c) $AA319 + 1\%\text{N}_{T6}$, d) $AA319 + 1\%\text{N}_{\text{OH}}$. In all cases, elemental analyses are listed and labeled as *Spectrum* and the studio number.

[15]. In the case of $AA319 + 2\%$Ni (Fig. 2e)), Al_3Ni in ribbon-like morphology was the most notable effect after Ni addition [16]. Ni intermetallics precipitated with Fe and Cu elements [17]. Microstructural changes due to $T6$ heat treatment were observed following the Oswald ripening process, a notable effect of coarsening and rounded ϵ-Si in $AA319_{T6}$ until remained some sharpest in $AA319+2\%\text{Ni}_{T6}$ (Fig. 2f)). Elemental analysis is included for phases commonly present in alloys in Fig. 2c), d) and g).

Regarding Cu clusters, there was a similar amount of Cu dissolved in α-Al after Ni addition, which remained without significant changes in both $AA319_{T6}$ and $AA319+2\%\text{Ni}_{T6}$. Additionally, in both solution temperatures schemes (495°C and 520°C), Cu clusters were maintained in similar amounts and sizes. The morphology of Al_9FeNi was modified in Ni

samples, differing from undesirable Fe phases with sharp edges.

Figure 3 characterized by TEM the evolution of micro- and nano- precipitates in $AA319$ and $AA319 + 1\%$Ni at $T6$ and over-heating thermal stages. $T6$ heat-treated samples in Figs. 3a) and 3c) show dark phases of irregular morphology, corresponding to high Si content precipitates with a similar composition range. $AA319_{T6}$ (Fig. 3a)) contains a high density of $Al_2Cu{-}\theta'$ precipitates in needle-like morphology. However, in $AA319 + 1\%Ni_{T6}$, the presence of needles-pairs with a relative angle of 90°C was increased, as seen in Fig. 3c). The average thickness of θ' in $AA319 + 1\%Ni_{T6}$ was close to 60%, a smaller amount than those needles contained in $AA319_{T6}$. Interestingly, even Ni and Cu's affinity at the nanoscale level is not observed as the dominant interaction to form Ni-Cu phases in competition with Al_2Cu needles.

The TEM micrograph presented in Fig. 3b) reveals that high temperatures, described in the experimental section, produce thermal degradation of the $AA319$. $AA319_{OH}$ sample shown in Fig. 3b) a representative area where θ' needles have been coarsened, retaining a minimal quantity in the matrix. In the evolution of the nanostructure of $AA319 + 1\%N_{OH}$, Fig. 3d) differs from $AA319_{OH}$ due to the higher amount of θ' phases. Even though θ' needles in $AA319 + 1\%N_{OH}$ retain the morphology and high aspect ratio, compared to T6 heat treated thermal state, they are coarser and retain a close and similar spatial distribution.

Figure 4 concentrates hardness and tensile test measures. The presence of hard Ni phases should be enough to increase hardness value regardless of thermal history; thus, this was observed since the as-cast condition, as seen in Fig. 4a). It was observed a gradual increment in hardness with Ni content additions in modified alloys. In the $T6$ condition, hardness variation is not significant since changes were just a few units. It was observed mechanical degradation by over-heated condition after high-temperature condition, with increment in hardness as a function of Ni content. The hardness of $AA319 + 2\%N_{OH}$ increased significantly from its previous thermal condition, $T6$. $AA319 + 1\%N_{OH}$ was enhanced around 10% relative to the reference alloy $AA319_{OH}$ and 5% compared to the maximum of $AA319_{T6}$.

In Fig. 4b, tensile tests are shown: in the as-cast condition, $AA319+1\%$Ni sample obtained the highest UTS values of 218 MPa, followed by $AA319$, +1.5%Ni, and +2%Ni (178 MPa). After $T6$ thermal treatment, $AA319 + 1.5\%Ni_{T6}$ and $AA319+1\%Ni_{T6}$ samples present the highest UTS values of 278 and 267 MPa, respectively. In comparison, the AA319 value was 246 MPa; over-heating conditions, the deteriorating effect in $AA319_{OH}$ and $AA319 + 1\%N_{OH}$ samples were evident. For the $AA319 + 1.5\%N_{OH}$ and $AA319 + 2\%N_{OH}$ samples, UTS values were 260 and 264 MPa, respectively, evidencing the effect of the addition of Ni. UTS reaches maximum values at the $T6$ stage for $AA319_{T6}$, $AA319{+}1\%N_{T6}$, and $AA319 + 1.5\%N_{T6}$; however, a pronounced drop of every maximum peak was observed in the over-heating condition. The maximum UTS was obtained at over-heating for $AA319 + 2\%N_{OH}$. UTS values until high-temperature conditions were maintained in the range of 136 MPa ($AA319 + 1\%N_{HT1}$) to 182 MPa ($AA319 + 2\%Ni_{HT1}$). Regarding the higher solubilized temperature, $HT2$, the range was 112 ($AA319 + 1\%N_{HT2}$) to 162 MPa ($AA319 + 2\%N_{HT2}$).

4. Discussion

Commercial aluminum alloy 319 (AA319) after $T6$ heat treatment reduced the amount and size of Cu clusters due to the solubilization process activated by high temperature [**?**]. In Ni-modified samples, a significant reduction in the size and quantity of mentioned Cu-clusters was presented. Regarding indexed crystal phases, XRD showed a quantity decrease in θ'-Al_2Cu due to Ni addition. Such results contrasted with TEM observations showing a higher density of θ' to all modified samples. This behavior can be attributed to XRD differences related to reducing the coarseness of θ' phases that precipitated in Ni samples. Ni phases formed in modified samples consisted of Al_3Ni, identified at the microscale

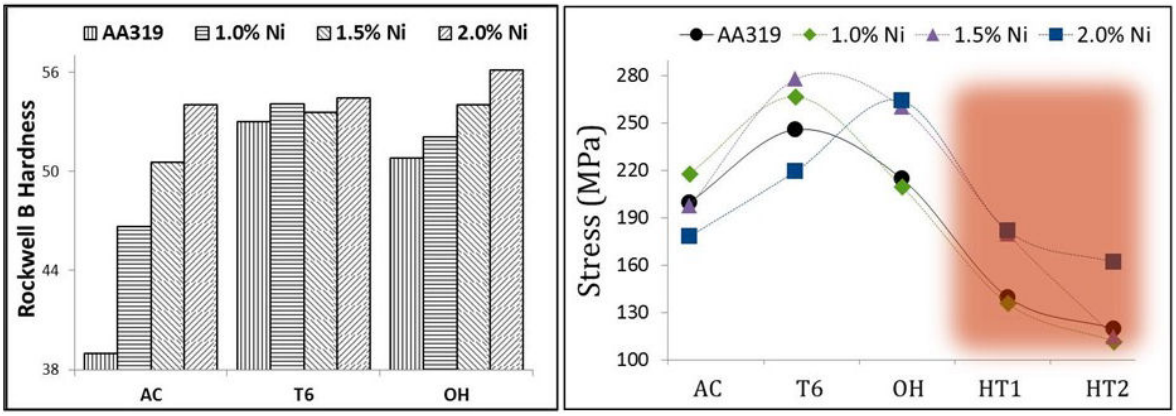

FIGURE 4. Rockwell B Hardness and UTS values for all chemical compositions;$AA319$, $AA319+1\%$Ni, $AA319+1.5\%$Ni, and $AA319+2\%$Ni. Used thermal stages were; as-cast, $T6$, over-aging, and high temperature for two different solubilization temperatures HT1 (495°C) and HT2 (520°C).

dimension and indexed by XRD. Ni precipitates must consist of a range of other reported phases. However, just Al_3Ni was in the range of XRD sensitivity. θ'-Al_2Cu dimensional reduction with the highest number of needles could improve UTS due to the highest number of obstacles to nanofractures diffusion. An essential difference between $AA319$ and Ni modified samples showed θ' needles in $AA319$ with higher density. In the case of Ni modified samples, there were precipitated in two different directions creating a high amount of θ' pairs. θ' mainly drove the hardness behavior until needle pairs were not influenced positively because of hardness depending on the global value of α-Al deformation. It can be rationalized that $T6$ results in θ' needles, which are the principal hardness enhancement, and Ni precipitates were screening contribution. The 250°C overheating conditions did not significantly modify the hardness values, and therefore, the presence of the Al_3Ni intermetallic was responsible for thermal stability. Due to that, a dynamic transformation was not observed; hardness decreased due to the coarsening of ϵ-Si and θ'-Al_2Cu phases. Hardness increased at the as-cast state was expected due to hard Ni precipitates in modified alloys. However, the $T6$ heat treatment condition and hardness behavior depended on θ' formation and presence as the principal hardness phase. Hardness decrement was observed at over-aging due to θ' phase coarsening as observed by TEM micrograph (Fig. 3b).

On the other hand, the retaining of θ' in Ni modified samples (Fig. 3d) was responsible for the favorable mechanical response. Copper-rich nanostructures were responsible for hardness enhancement. Thus Ni precipitates attenuated detrimental effect on UTS due to the increasing number of θ'-Al_2Cu needles. After the high-temperature event, the maximum hardness of $AA319 + 2\%N_{OH}$ could be reasonable to reduce θ'-Al_2Cu kinetics of precipitation by Ni presence.

The mechanism, such as Ni interacting with Cu to reduce the size of the needles, was not clear after using TEM micrographs at solubilized samples after 1 to 4 hrs. However, it was supposed a reduction of kinetics transformation from GP to θ'. Thin needles precipitated due to Ni additions under the same heat treatment as $AA319_{T6}$, however, coarsening of θ' at 250°C occurred at all samples. Improvement of Ni samples was because the size of needles was smaller before starting the high temperature, thereby delaying the alloy's deterioration.

Al-Ni precipitates are hard and brittle particles, which can decrease UTS in the way that occurred in $AA319 + 2\%N_{AC}$. However, the increase of Al_2Cu phases positively counterbalanced the presence of Ni phases in a significant way. UTS value increased by Ni addition due to the higher density of Al_2Cu with a smaller dimension. The observed drop in UTS values at high temperatures and long times is due to the coarsening of Al-Cu and Al-Si precipitates, which quickly screen the improvements done by Ni precipitates. It is a known fact that the coarsening of Al_2Cu phases is presented as a function of the temperature. However, the detrimental effect of transformation kinetics of the θ' phase in this condition was attenuated mainly in the $AA319 + 1\%N_{OH}$ sample.

5. Conclusion

Commercial aluminum alloy 319 and a series of alloys modified with $+1.0\%$, $+1.5\%$, and $+2.0\%$ Nickel were used to investigate their micro and nanostructural evolution. The synthesized conditions were as-cast, $T6$, overheating, and high temperature. By TEM micrographs, it was concluded that the modified alloys reduce θ'-Al_2Cu precipitation kinetics in comparison to the commercial alloy. The direct effect of Ni additions on mechanical properties was an increase in both hardness and UTS. In the latter case, the maximum UTS values at $T6$ were for $AA319 + 1.5\%$Ni addition, followed by $AA319 + 1.0\%$Ni. After being subjected to 250°C for 30 minutes, the $AA319 + 1.5\%$Ni alloy was the only one that preserved the mechanical conditions for engineering applications. Compared to the tests performed on the material at 250°C, the alloy $AA319 + 2\%$Ni was the least affected, confirming the reduction of θ'-Al_2Cu phase kinetics.

Acknowledgments

The authors are grateful to CONACYT for 290674 and 290604 scholarships. This research work was carried out during the summer research internship at UACH-COMIMSA-2021.

1. V. Chak, H. Chattopadhyay, and T. L. Dora, A review on fabrication methods, reinforcements and mechanical properties of aluminum matrix composites, *Journal of Manufacturing Processes* **56** (2020) 1059, https://doi.org/10.1016/j.jmapro.2020.05.042.

2. T. P. Hovorun, K. V. Berladir, V. I. Pererva, S. G. Rudenko, A. I. Martynov, Modern materials for automotive industry, *Journal of Engineering Sciences* **4** (2017) 8, https://doi.org/10.21272/jes.2017.4(2).f8.

3. A. Contreras, E. Bedolla, Fabricación y caracterización de materiales compuestos de matriz metálica Al-Cu y Al-Mg reforzados con partículas de tic, *Rev. Mex. Fis* **50** (2004) 495.

4. T. Kobayashi, Strength and fracture of aluminum alloys, *Materials Science and Engineering: A* **280** (2000) 8, https://doi.org/10.1016/S0921-5093(99)00649-8

5. M. Becerril, O. Vigil-Galán, G. Contreras-Puente, and O. Zelaya-Angel, Aluminum doping of cdte polycrystalline films starting from the heterostructure cdte/al, *Rev. Mex. Fis* **57** (2011) 304.

6. H. Ramezanalizadeh, and S. R. Iyzi, Fabrication and hardness investigation of Al-15%mg2Si-3%Cu in-situ cast composite, Advances in *Materials and Processing Technologies* **0** (2021) 1, https://doi.org/10.1080/2374068X.2021.1909331.
7. X. Deng, Precipitation strengthening of stress-aged al-cu-mg-ag alloy single crystals, *Materials Science and Engineering: A* **819** (2021) 141458. https://doi.org/10.1016/j.msea.2021.141458.
8. S. Amirkhanlou and S. Ji, Casting lightweight stiff aluminum alloys: a review, *Critical Reviews in Solid State and Materials Sciences* **45** (2020) 171, https://doi.org/10.1080/10408436.2018.1549975.
9. M. F. Ibrahim, A. M. Samuel, H.W. Doty, and F. H. Samuel, Effect of aging conditions on precipitation hardening in al-si-mg and al-si-cu-mg alloys, *International Journal of Metalcasting* **11** (2017) 274, https://doi.org/10.1007/s40962-016-0057-z.
10. A. Girgis, M. H. Abdelaziz, A. M. Samuel, S. Valtierra, and F. H. Samuel, On the enhancement of the microstructure and tensile properties of an alâcu based cast alloy, *Metallography, Microstructure, and Analysis* **8** (2019) 757, https://doi.org/10.1007/s13632-019-00583-8.
11. M. A. Hussein, S. H. Al-Shafaie, and N. S. Radhi, Preparation and investigation physical properties of functionally graded materials of aluminum-nickel alloys, *Journal of Physics: Conference Series* **1999** (2021) 012067. https://doi.org/10.1088/1742-6596/1999/1/012067.
12. S. Madhankumar, K. Sivakumar, J. Chandradass, R. Srinivasa-Addanki, V. Alphonse-Rodriguez, and U. Saroshkumar, Materials Today: Proceedings. International Conference on Mechanical, Electronics and Computer Engineering 2020: *Materials Science* **45** (2021) 6852, https://doi.org/10.1016/j.matpr.2020.12.1030.
13. T. Klein, C. Pauly, F. Mucklich, and G. Kickelbick, Al and ni nanoparticles as precursors for ni aluminides, *Intermetallics* **124** (2020) 106839. https://doi.org/10.1016/j.intermet.2020.106839.
14. A. Kumar, V. Kukshal, and V. R. Kiragi, Assessment of mechanical and sliding wear performance of ni particulate filled 7075 aluminium alloy composite, *Materials Today: Proceedings* **44** (2021) 4349, https://doi.org/10.1016/j.matpr.2020.10.556.
15. L. Alyaldin, M. H. Abdelaziz, A. M. Samuel, H. W. Doty, and F. H. Samuel, Effect of transition metals addition on tensile properties of alâsiâcu-based alloys at 25 c and 250 c: Role of heat treatment, *Inter Metalcast* **15** (2021) 60, https://doi.org/10.1007/s40962-020-00427-0.
16. M. S. Kaiser, S. H. Sabbir, M. S. Kabir, M. R. Soummo, and M. A. Nur, Study of mechanical and wear behaviour of hypereutectic al-si automotive alloy through fe, ni and cr addition, *Materials Research* **21** (2018) 0. https://doi.org/10.1590/1980-5373-MR-2017-1096.
17. Z. Yang *et al*., Diffusion bonding of ni3al-based alloy using a ni interlayer, *Journal of Alloys and Compounds* **819** (2020) 153324. https://doi.org/10.1016/j.jallcom.2019.153324.
18. S. Nallusamy, A review on the effects of casting quality, microstructure and mechanical properties of cast al-si-0.3mg alloy, International *Journal of Performability Engineering* **12** (2016) 143, https://doi.org/10.23940/ijpe.16.2.p143.mag.